

# Madden-Julian Variability in Coupled Models

Kenneth R. Sperber<sup>1</sup>, Silvio Gualdi<sup>2</sup>, Wei Li<sup>3</sup> and Julia M. Slingo<sup>4</sup>

<sup>1</sup>Program for Climate Model Diagnosis and Intercomparison, Lawrence Livermore National Laboratory, P.O. Box 808, L-264, Livermore, CA 94550 USA (sperber1@llnl.gov)

<sup>2</sup>National Institute of Geophysics and Volcanology, Via Gobetti 101, 40129 Bologna, Italy

<sup>3</sup>LASG, Institute of Atmospheric Physics, P.O. Box 9804, Beijing 100029, China

<sup>4</sup>Centre for Global Atmospheric Modelling, Dept. of Meteorology, University of Reading, P. O. Box 243, Reading RG6 6BB, England

## 1. Introduction

The Madden-Julian Oscillation (MJO) is a dominant mode of tropical variability (Madden and Julian 1971, 1972). It is manifested on a timescale of ~30-70 days through large-scale circulation anomalies which occur in conjunction with eastward propagating convective anomalies over the eastern hemisphere. Recent evidence has suggested that an interactive ocean may be important for the simulation of the Madden-Julian Oscillation (Flatau et al. 1997, Sperber et al. 1997, Waliser et al. 1999, Inness et al. 2002). As part of an initiative to the CLIVAR Working Group on Coupled Modelling, we examine ocean-atmosphere GCMs to ascertain the degree to which they can represent the 4-dimensional space-time structure of the MJO. The eastward propagation of convection is also examined with respect to the surface fluxes and SST, and we compare and contrast the behavior over the Indian Ocean and the western Pacific. Importantly, the results are interpreted with respect to systematic error of the mean state.

## 2. The Models

Here we analyze 10 years of daily data from the coupled model from the Institute of Atmospheric Physics. This model, known as GOALS (Global Ocean-Atmosphere-Land System), consists of an R15 atmospheric GCM with 9 vertical levels, and an ocean model with a horizontal resolution of  $4^\circ \times 5^\circ$  with 20 vertical levels. Further details of this model, including aspects of its intraseasonal variability are discussed in Li and Yu (2000).

20 years of daily data from the SINTEX coupled model are analyzed. This model consists of a T30 L19 version of ECHAM4 (Roeckner et al. 1996) and the ORCA ocean GCM (Madec et al. 1998) with horizontal resolution of  $2^\circ \times 1.5^\circ$  ( $0.5^\circ$  near the equator) with 31 vertical levels.

The NCEP/NCAR reanalysis (Kalnay et al. 1996) and AVHRR OLR (Gruber and Winston 1978, Gruber and Krueger 1984) for the period 1982-1991 are used as validation data. This period was chosen since the weekly SST (interpolated to daily) were used as the surface boundary condition for the reanalysis. Prior to December 1981 only monthly SST were available which would have compromised the isolation of intraseasonal variations in SST.

## 3. Intraseasonal Variability

Here, the spatio-temporal evolution of the MJO is keyed to the development of the convective anomalies. We use EOF analysis of 20-100 day bandpass filtered AVHRR and simulated OLR over the region  $45^\circ\text{E}-120^\circ\text{W}$ ,  $20^\circ\text{S}-20^\circ\text{N}$  for the months November-March. For the models and observations, EOF-1 is associated with enhanced convection over the Maritime continent. In conjunction with EOF-2 (EOF-2 and EOF-3 in the case of the SIN-

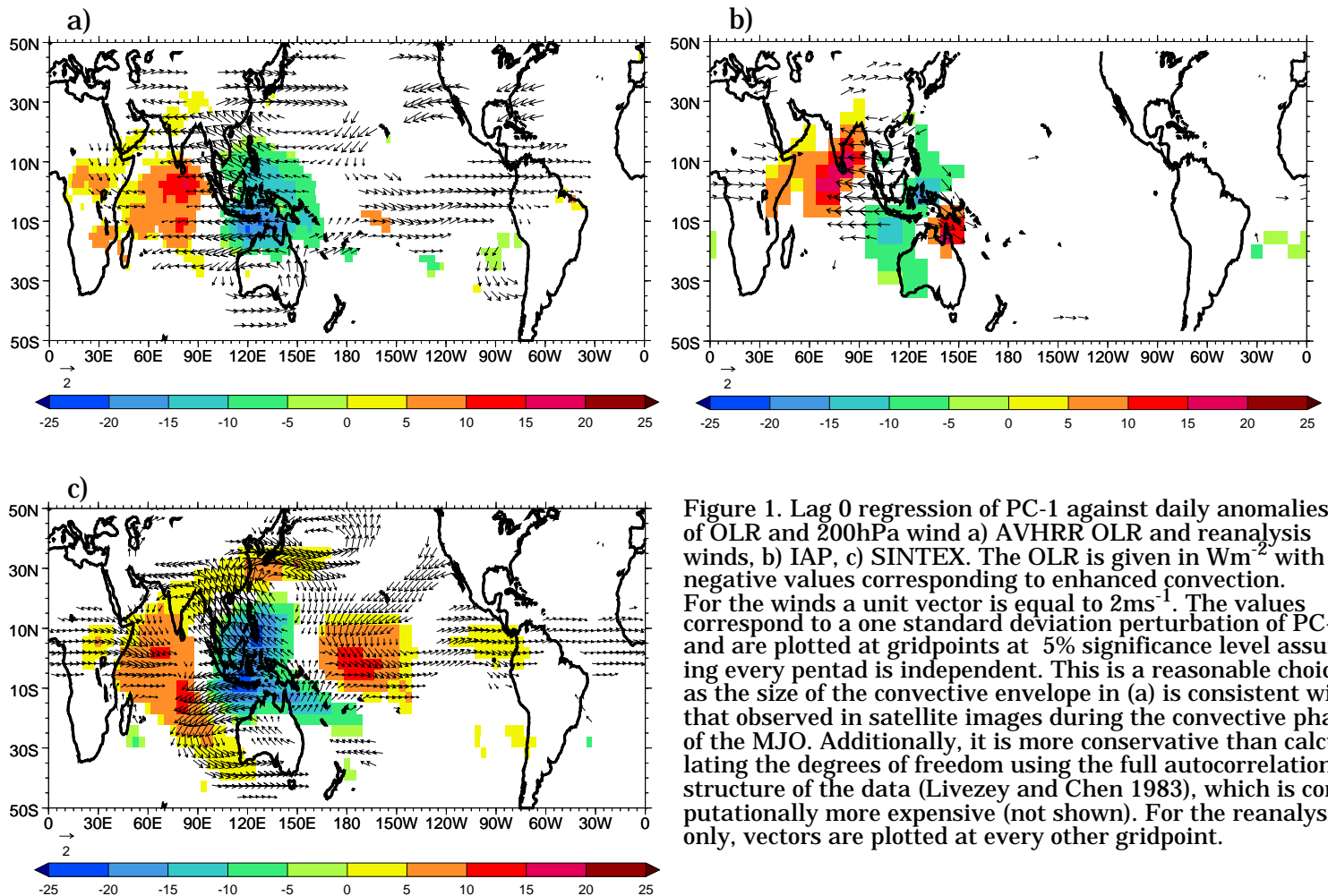


Figure 1. Lag 0 regression of PC-1 against daily anomalies of OLR and 200hPa wind a) AVHRR OLR and reanalysis winds, b) IAP, c) SINTEX. The OLR is given in  $\text{Wm}^{-2}$  with negative values corresponding to enhanced convection. For the winds a unit vector is equal to  $2\text{ms}^{-1}$ . The values correspond to a one standard deviation perturbation of PC-1, and are plotted at gridpoints at 5% significance level assuming every pentad is independent. This is a reasonable choice as the size of the convective envelope in (a) is consistent with that observed in satellite images during the convective phase of the MJO. Additionally, it is more conservative than calculating the degrees of freedom using the full autocorrelation structure of the data (Livezey and Chen 1983), which is computationally more expensive (not shown). For the reanalysis only, vectors are plotted at every other gridpoint.

TEX model) these leading modes capture the eastward propagation of the MJO related convection from the Indian Ocean to the central Pacific and into the SPCZ (not shown). The associated principal component (PC) time series are dominated by timescales of 30-70 days (not shown) indicating that the models have a realistic periodicity in their MJO activity.

For the leading mode, PC-1 has been regressed against (unfiltered) daily anomalies of many fields to capture the spatio-temporal evolution of the MJO. In Fig. 1, PC-1 has been regressed against anomalies of OLR and the winds at 200hPa at zero time lag. As seen in Fig. 1a, the observed convective envelope covers the Maritime continent with the strongest convective anomalies,  $\sim 20\text{Wm}^{-2}$ , occurring near  $7^{\circ}\text{S}$ . The dominant upper-level outflow occurs at and to the west of the convection, and is seen as easterly wind anomalies at 200hPa. Further poleward, the forced Rossby wave response is seen as anticyclonic wind anomalies, while further east cyclonic anomalies are evident. To the west of the enhanced convection, there is upper-level convergence and suppressed convection over the western/central Indian Ocean. The SINTEX model captures these features realistically, though this model has a much stronger than observed meridional wind component associated with the convection. The IAP model underestimates the magnitude of the convective anomalies, which do not have as great a longitudinal extent as observed. Additionally, the Rossby wave response is not as robust as observed.

The regressions have been calculated for time lags of  $\pm 25$  days to examine the propagation of the MJO. To concisely show the propagation, we plot fields of interest as a function of longitude and time lag at a specific latitude, as seen for observations and reanalysis in Fig. 2. The latitude of interest is about  $7^{\circ}\text{S}$ , where the anomalies tend to be strongest.

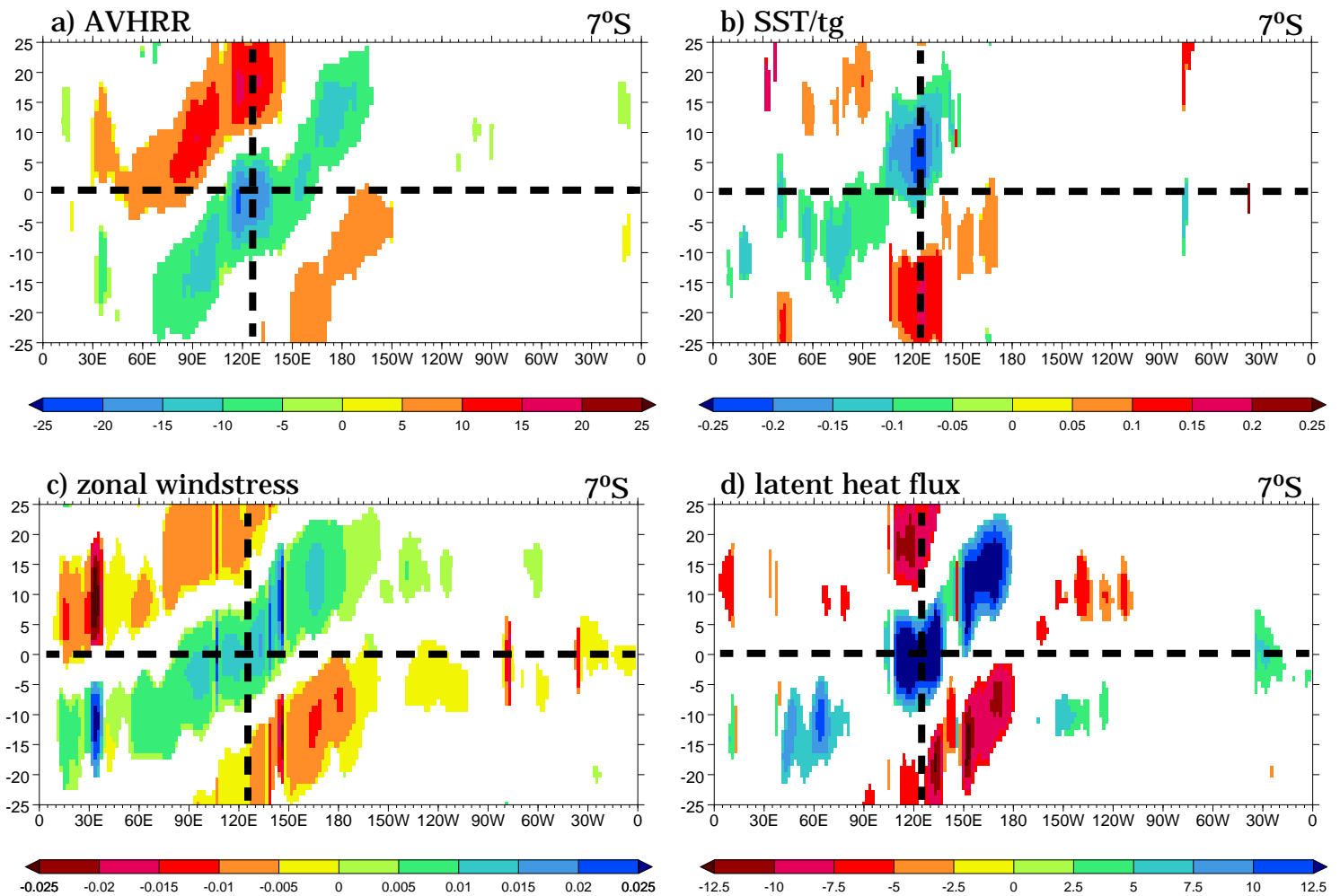


Figure 2. Regressions of PC-1 against unfiltered daily anomalies of a) AVHRR OLR ( $\text{Wm}^{-2}$ ), b) SST and reanalysis ground temperature ( $^{\circ}\text{C}$ ), c) reanalysis zonal windstress ( $\text{Nm}^{-2}$ ), and d) reanalysis latent heat flux ( $\text{Wm}^{-2}$ ). The values correspond to a 1 standard deviation perturbation of PC-1. The vertical dashed line corresponds to the longitude where the strongest convective anomalies occur (Fig. 1a). The horizontal dashed line corresponds to zero time lag.

First we will discuss the behaviour near  $125^{\circ}\text{E}$  where EOF-1/PC-1 have the maximum projection. As seen in Fig. 2a, convection begins at  $125^{\circ}\text{E}$  at about day -10. Prior to day -15 the zonal windstress anomalies are easterly (Fig. 2c), and as such the latent heat flux is weaker than normal (Fig. 2d). This, in conjunction with enhanced shortwave radiation at the surface (not shown), gives rise to above normal SST near the Maritime continent prior to the onset of convection, consistent with the results of Sperber et al. (1997) and Woolnough et al. (1999). From day -10 through day +5 the convection is strong near  $125^{\circ}\text{E}$ . During this time the westerly windstress anomalies are associated with enhanced latent heat flux (Fig. 2d) and below normal shortwave radiation at the surface (not shown), with the integrated effect being the below normal SST that persists through day +15.

With respect to the eastward propagation, the convection begins near  $65^{\circ}\text{E}$  about 25 days prior to the maximum over the Maritime continent. From the Indian Ocean to the Maritime continent the propagation rate remains uniform. Over the Maritime continent the eastward propagation stalls somewhat until about day +5 when the uniform eastward propagation is again seen. Initially, the westerly windstress anomalies over the Indian Ocean develop subsequent to the convective anomalies, with the westerlies tending to be located to the west of the convection. However, from about day -15 onward, the westerlies underlie the convective anomalies.

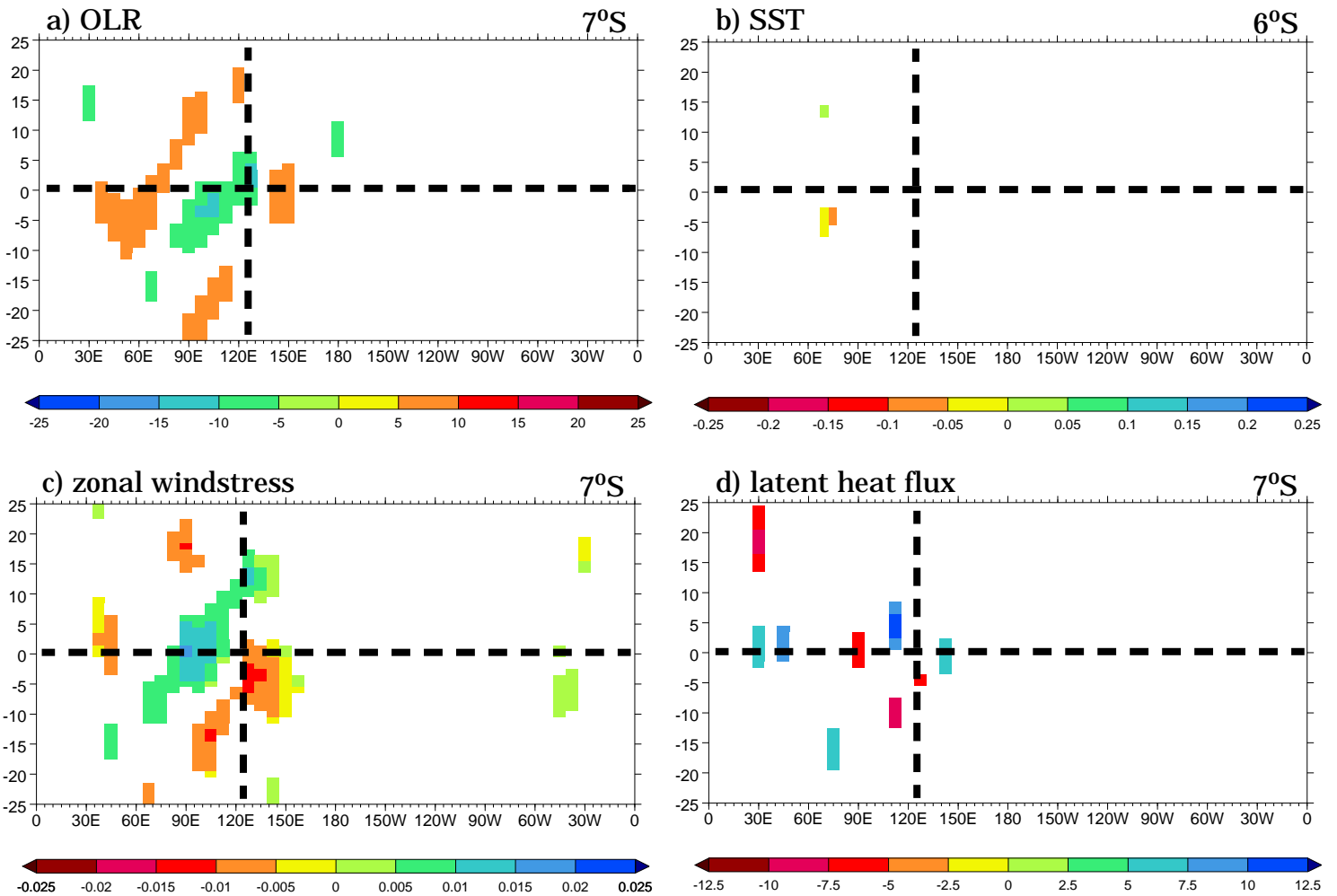


Figure 3. As Fig. 2 but from the IAP model.

As seen in Figs. 3a and 3c, the IAP model shows coherent eastward propagation of OLR and zonal windstress anomalies, though the anomalies fail to propagate east of the Maritime continent. Additionally, the model does not capture the strong links to the SST and latent heat flux (Figs. 3b and 3d) seen in the reanalysis/observations.

The SINTEX model captures many of the major features of the observed propagation, though differences in detail exist (Fig. 4). For example, during the onset of convection in the Indian Ocean the zonal windstress (Fig. 4c) underlies the convection (Fig. 4a), unlike the reanalysis/observations. Near 160°E, the eastward propagation of enhanced convection ceases, and the model has a pronounced standing oscillation east of the dateline. With the lack of coherent eastward propagation of convection in the western Pacific, the model does not capture the enhanced latent heat flux there during positive time lags (Fig. 4d). Importantly, the model does capture the warming near 120°E that occurs prior to the onset of convection (Fig. 4b), and the subsequent cooling from the enhanced latent heat flux.

#### 4. Relation to Systematic Model Error

The MJO projects strongly on to the zonal wind (Slingo et al. 1996, 1999), and here we examine the November-March windstress climatologies to search for a link between the mean state and the ability to capture intraseasonal variations. As seen in Fig. 5a, the near-equatorial Indian Ocean and western Pacific is characterized by a broad region of westerlies. This coincides with the region over which eastward propagation of MJO convection occurs. For the IAP model (Fig. 5b), consistent with the lack of eastward propagating in-

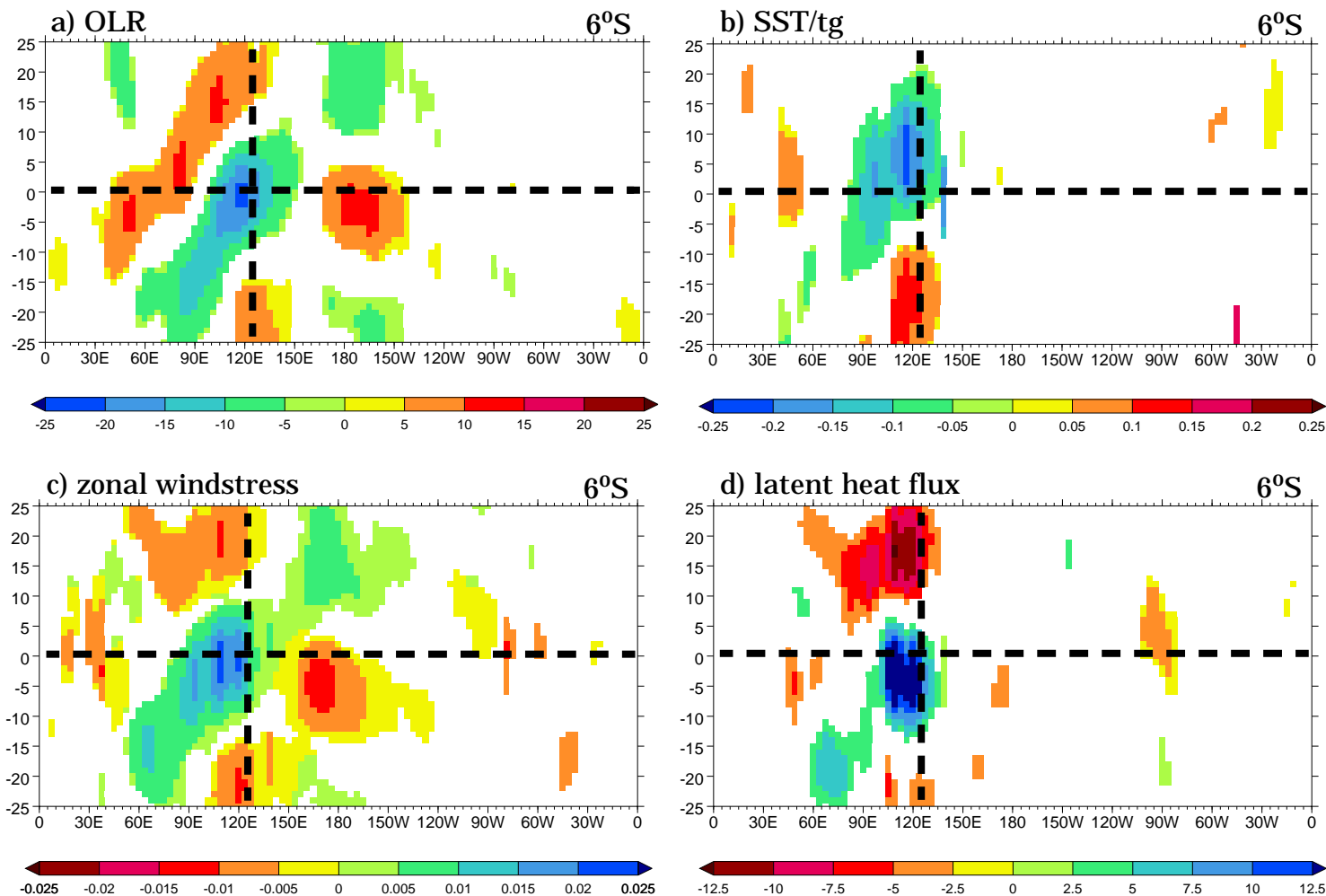


Figure 4. As Fig. 2 but from the SINTEX model.

traseasonal convection from 140°E eastward, the time mean zonal wind stress is easterly over the western Pacific. For the SINTEX model (Fig. 5c), the zonal wind stress climatology has westerlies over the Indian Ocean and Maritime continent, and westerlies east of 150°E. These regions are separated by a narrow zone of easterlies between 140-150°E which distinguishes the eastward propagating convective regime to the west, and the standing convective signature to the east. These findings from models and reanalysis extend into the lower troposphere, also being seen at 850hPa (not shown). Furthermore, the relationship between the systematic error in the zonal component of the wind and the intraseasonal convection is consistent with that found in HADCM3 (Inness and Slingo 2002).

## 5. Summary

The ability of two coupled models to represent MJO-like variability has been evaluated, and the quality has been linked to systematic error of the mean state. Both models are most realistic over the Indian Ocean. The SINTEX model better simulates the coherence of the eastward propagation of convection, and the link to the surface fluxes, but it also has an overly strong meridional wind signature. Both models do not capture the eastward propagation over the western Pacific, with the IAP model failing to have a statistically significant signature, and the SINTEX model producing a standing oscillation near the date-line, unlike the observations.

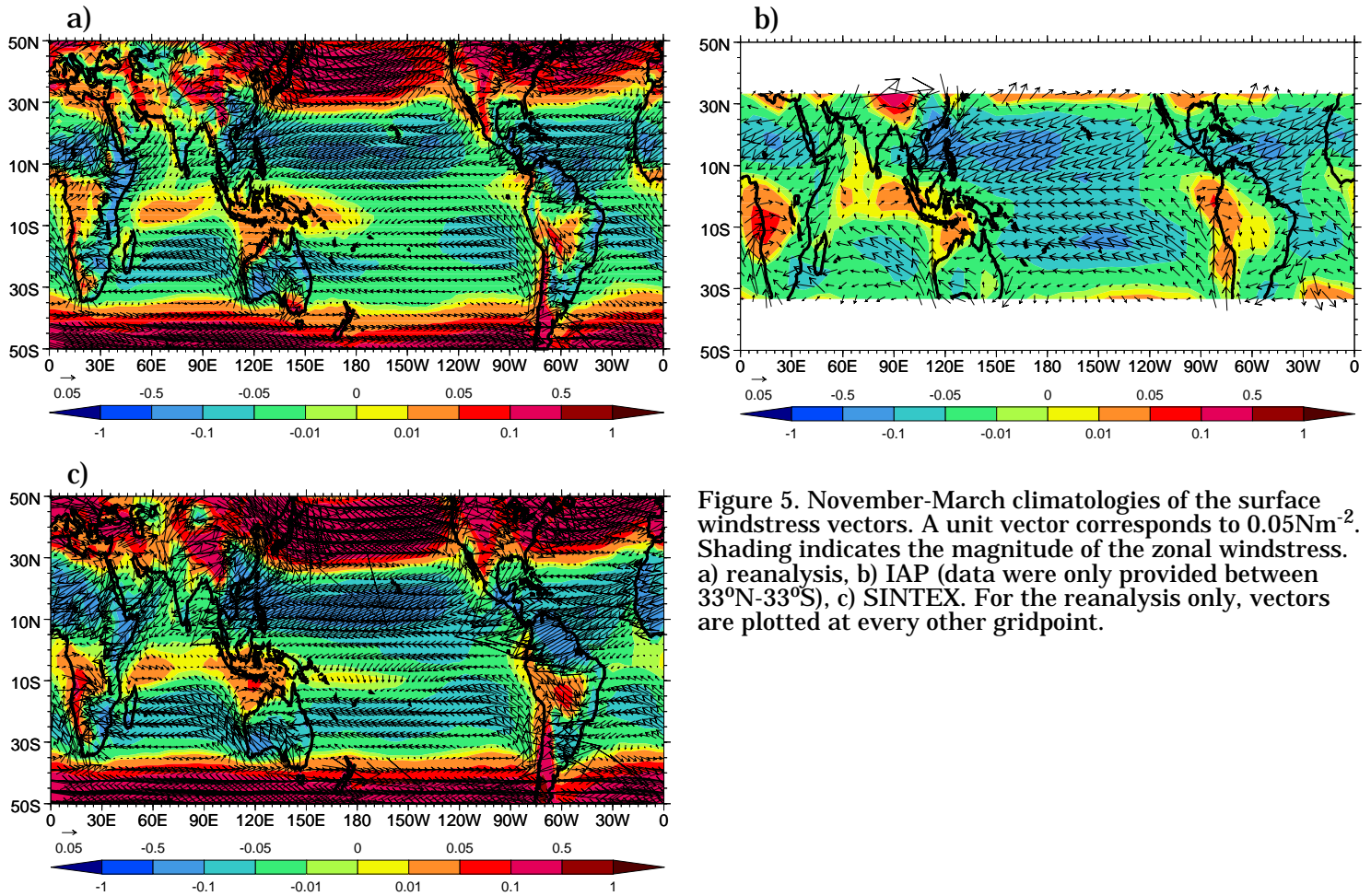


Figure 5. November-March climatologies of the surface windstress vectors. A unit vector corresponds to  $0.05\text{Nm}^{-2}$ . Shading indicates the magnitude of the zonal windstress. a) reanalysis, b) IAP (data were only provided between  $33^{\circ}\text{N}$ - $33^{\circ}\text{S}$ ), c) SINTEX. For the reanalysis only, vectors are plotted at every other gridpoint.

*Acknowledgments.* This work was performed under the auspices of the U.S. Department of Energy at the University of California Lawrence Livermore National Laboratory under contract No. W-7405-Eng-48. K. R. Sperber gratefully acknowledges the support of the Centre for Global Atmospheric Modelling and Dept. of Meteorology at the University of Reading, England, at which a portion of this work was completed.

## References

- Flatau, M, P. J. Flatau, P. Phoebus, and P. P. Niiler, 1997: *JAS*, 54, 2373-2386.  
 Gruber, A. and J. S. Winston, 1978: *BAMS*, 59, 1570-1573.  
 Gruber, A. and A. F. Krueger, 1984: *BAMS*, 65, 958-962.  
 Inness, P. M., J. M. Slingo, 2002: *J. Clim.* (submitted)  
 Inness, P. M., J. M. Slingo, E. Guilyardi, and J. Cole, 2002: *J. Clim.* (submitted)  
 Kalnay, E, M. Kanamitsu, R. Kistler, W. Collins, D. Deaven, L. Gandin, M. Iredell, S. Saha, G. White, J. Woollen, Y. Zhu, M. Chelliah, W. Ebisuzaki, W. Higgins, J. Janowiak, K.-C. Mo, C. Ropelewski, J. Wang, A. Leetmaa, R. Reynolds, R. Jenne, and D. Joseph, 1996: *BAMS*, 77, 437-471.  
 Li, W and Y. Yu, 2000: *Chinese JAS*, 24, 344-358.  
 Livezey, R. E. and W. Y. Chen, 1983: *MWR*, 111, 46-59.  
 Madden, R. A. and P. R. Julian, 1971: *JAS*, 28, 702-708.  
 Madden, R. A. and P. R. Julian, 1972: *JAS*, 29, 1109-1123.  
 Madec, P. Delecluse, M. Imbard, and C. Levy, 1998: *LODYC/IPSL Note 11*, 91pp.  
 Roeckner, E., K. Arpe, L. Bengtsson, M. Christoph, M. Claussen, L. Dümenil, M. Esch, M. Giorgetta, U. Schlese, U. Schulzweida, 1996: *MPI Report No. 218*, 90pp.  
 Slingo, J. M., K. R. Sperber, J. S. Boyle, J.-P. Ceron, M. Dix, B. Dugas, W. Ebisuzaki, J. Fyfe, D. Gregory, J.-F. Gueremy, J. Hack, A. Harzallah, P. Inness, A. Kitoh, W. K.-M. Lau, B. McAvaney, R. Madden, A. Matthews, T. N. Palmer, C.-K. Park, D. Randall, and N. Renno, 1996: *Clim. Dyn.*, 12, 325-357.  
 Slingo, J. M., D. P. Rowell, K. R. Sperber, and F. Nortley, 1999: *QJRMS*, 125, 583-609.  
 Sperber, K. R., J. M. Slingo, P. M. Inness, and W. K.-M. Lau, 1997: *Clim. Dynam.*, 13: 769-795.  
 Waliser, D. E., K.-M. Lau, and J.-H. Kim, 1999: *JAS*, 56, 333-358.  
 Woolnough, S. J., J. M. Slingo, and B. J. Hoskins, 1999: *J. Clim.*, 13, 2086-2104.